Effect of Cation Complexation on the Structure of a Conformationally Flexible Multiply Charged Anion: Stabilization of Excess Charge in the $Na^+ \cdot$Adenosine 5′-Triphosphate Dianion Ion-Pair Complex

Ruth M. Burke and Caroline E. H. Dessent*

Department of Chemistry, University of York, Heslington, York YO10 5DD, U.K.

Received: July 3, 2008; Revised Manuscript Received: January 19, 2009

We report a computational study of the conformationally and tautomerically flexible cation−dianion complex of Na^+ with doubly deprotonated adenosine 5′-triphosphate (ATP) using a hierarchical selection method. The method uses molecular dynamics to generate initial conformeric structures, followed by a classification process that groups conformers into five "families" to ensure that a representative sample of structures is retained for further analysis, while very similar conformational structures are eliminated. Hierarchical ab initio calculations (DFT and MP2) of typical conformers of the families are then performed to identify the lowest-energy conformeric structures. The procedure described should provide a useful methodology for conducting higher-level ab initio calculations of medium-sized gas-phase biological molecules for interpreting contemporary laser spectroscopy measurements. For $Na^+ \cdot [ATP\text{-}2H]^2$ (considering tautomers where the phosphate chain of ATP is doubly deprotonated), the calculations reveal that the sodium cation interacts directly with the negatively charged phosphates (maximum distance = 2.54 Å) in all of the low-energy conformers, while a number of the structures also display close cation−adenine interactions producing compact ball-like structures. These compact structures generally correspond to the lowest-energy conformers. The structural variation between the bare $[ATP\text{-}2H]^{2-}$ molecular ion (Burke et al. *J. Phys. Chem. A* 2005, *109*, 9775−9785) and the $Na^+ \cdot [ATP\text{-}2H]^{2-}$ cluster is discussed in detail, including the effect of sodiation on the intramolecular hydrogen-bonding network within ATP in a gas-phase environment.

1. Introduction

The study of isolated gas-phase biological molecules has developed into a rapidly expanding field of research over recent years, with much experimental and theoretical effort being expended to provide detailed insights into the geometric and electronic properties of these important molecules.[1−16] Much of this research effort is driven by the challenge of understanding the factors that control the geometric structure of these conformationally flexible systems within the gas-phase environment where the intrinsic structures are not affected by interactions with solvent molecules or counterions.[3] The effect of solvent (or counterions) on the molecular structure can then be investigated through the study of molecular clusters.[1] Such an approach follows the tradition of gas-phase cluster studies of smaller molecular systems, where considerable progress has been made in understanding the detailed nature of solvation effects on both spectroscopic and thermodynamic parameters.[17−20] An important aspect of such gas-phase studies of isolated molecular species is that they provide crucial benchmarking data for assessing the reliability of computational approaches to molecular structure determination. Indeed, there is a strong synergy between high-level computational chemistry and gas-phase high-resolution laser spectroscopic studies, in particular, since accurate calculations are essential for interpreting the spectra obtained.[21]

In this paper, we report a computational study of the effect of cation complexation on the conformationally flexible gas-phase ion, doubly deprotonated adenosine 5′-triphosphate (ATP), i.e., $Na^+ \cdot [ATP\text{-}2H]^{2-}$. The work presented here builds on our earlier study of the bare $[ATP\text{-}2H]^{2-}$ dianion,[22] where we specifically focused on the dianionic species formed when two protons of the phosphate chain have been removed. In that study, the extent of intramolecular hydrogen bonding was found to be the primary factor determining the relative stability of the various conformational isomers of the gas-phase ion. Our focus in this work is on understanding the preferred binding sites for the Na^+ cation to the same doubly deprotonated $[ATP\text{-}2H]^{2-}$ dianion, and how complexation of $[ATP\text{-}2H]^{2-}$ with Na^+ affects the intramolecular hydrogen-bonding within the ATP ion in a gas-phase environment. There are currently very few detailed gas-phase experimental or computational studies of mixed charge (i.e., ion pair) systems containing biological molecules.[23−25] We note that Julian and Beauchamp have investigated collisional activation of sodiated clusters of deprotonated adenosine 5′-monophosphate to model abiotic ATP synthesis.[14]

The calculation of the lowest-energy geometric structures for a system such as $Na^+ \cdot [ATP\text{-}2H]^{2-}$ is nontrivial, since the $[ATP\text{-}2H]^{2-}$ dianion has four possible tautomers associated with deprotonation of the phosphate chain (Figure 1) in addition to considerable conformational flexibility. We explore the tautomeric and conformational space of our $Na^+ \cdot [ATP\text{-}2H]^{2-}$ system by using molecular dynamics to generate initial conformeric structures and then performing hierarchical ab initio calculations of selected conformers to obtain a fuller picture of the conformational potential energy surface. This procedure has the advantage of retaining a representative sample of structures for higher-level analysis while eliminating very similar conformational structures, thus reducing the number of unnecessary calculations.

* Corresponding author. Fax: 44-1904-432516. E-mail: ced5@york.ac.uk.

10.1021/jp805868u CCC: $40.75
Published on Web 02/27/2009

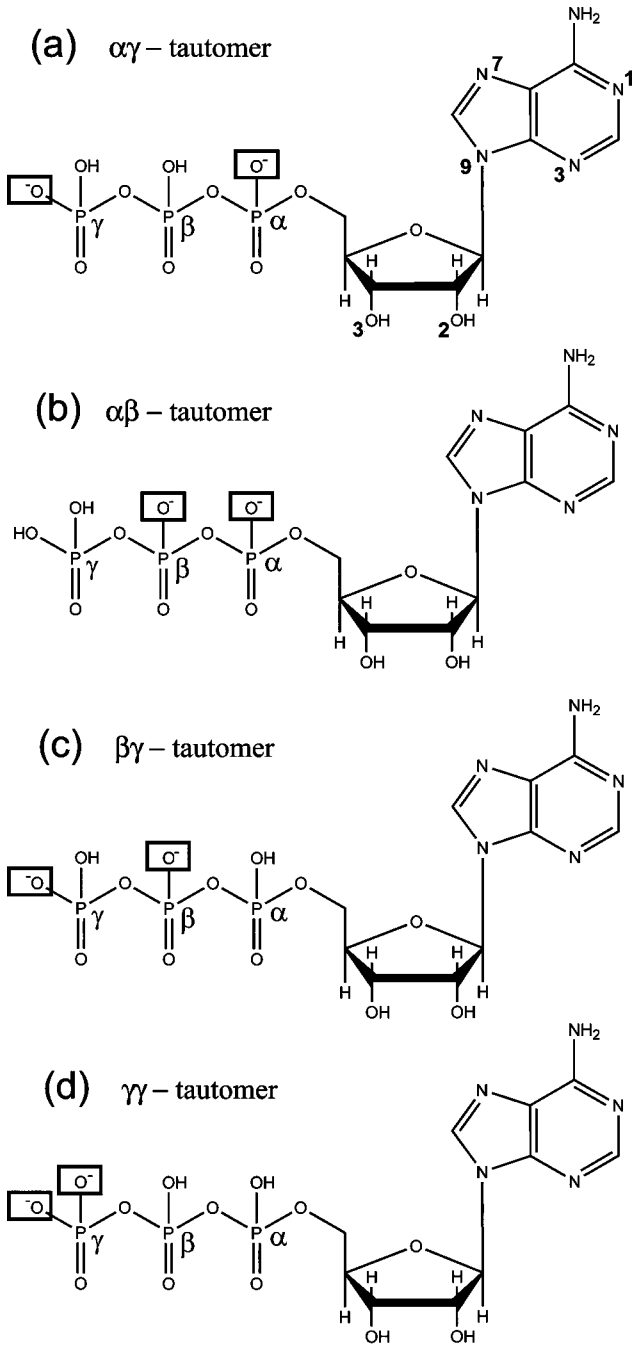

Figure 1. Chemical structures of the tautomers of doubly deprotonated ATP, i.e., $[ATP\text{-}2H]^{2-}$ where two protons from the phosphate chain have been removed: (a) $\alpha\gamma$- (b) $\alpha\beta$- (c) $\beta\gamma$-, and (d) $\gamma\gamma$-tautomer, where the α, β, and γ labels refer to the phosphate group(s). The labeling scheme for the nitrogen atoms of adenine is also illustrated.

Previous gas-phase studies of ground-state ion pairs have focused on systems where the conformational space is almost entirely restricted.[26−31] (We exclude ion pairs that are excited electronic states, i.e., charge-transfer states[32,33] and solvent-induced ion pairs, from this discussion.[34]) For ion pairs that consist of dianion−cation complexes, we have investigated simple complexes such as $K^+ \cdot Pt(CN)_4^{2-}$ and found that the metal ion only weakly perturbs the electronic structure of the multiply charged anion.[26,27] Wang and co-workers have used photodetachment photoelectron spectroscopy to probe the $Li^+ \cdot B_6^{2-}$ and $Na^+ \cdot SO_4^{2-}$ clusters.[28,29] The only gas-phase structural study of comformationally flexible dianion−cation complexes that we are aware of was conducted by Barran and co-workers,[23] who used ion-mobility mass spectrometry to investigate $Na^+ \cdot$oligosaccharide anion complexes. A separate class of studies have investigated the formation of zwitterions within cationized amino acid complexes, although these studies are distinctive since the presence of the cation promotes the zwitterionic state.[24,25] Mixed-charge clusters are, of course, common species in both electrospray ionization and MALDI mass spectrometry, where they are generally viewed as species that complicate the spectrum of the chemical system under investigation.[35]

To provide some biological context, in aqueous solution, the four pK_a values associated with the acidic protons of the phosphate of ATP are $\ll 1$ for the protons at the α and β phosphates (Figure 1), $\sim$1.0 for the first proton removed from the γ phosphate, and 6.5 for the second proton at the γ phosphate group.[36,37] The pK_avalue of the N1 position (4.0) is also of relevance, so that in solution "neutral" ATP is actually a zwitterionic species with either the α or β phosphate group deprotonated and the N1 group protonated.[36,37] The $[ATP\text{-}2H]^{2-}$ species in aqueous solution should therefore also be protonated at the N1 position, with deprotonation at the α and β phosphate groups, and single deprotonation at the γ phosphate group.[38] The $Na^+ \cdot [ATP\text{-}2H]^{2-}$ system studied in this work should therefore be viewed as a model mixed-charge species rather than a species with direct biological relevance. However, the methodology presented here could be readily extended for performing detailed computational studies of the biologically important species, e.g. $(Na^+)_2 \cdot [ATP\text{-}4H]^{4-}$ and $Mg^{2+} \cdot [ATP\text{-}4H]^{4-}$.[38,39] Such studies have the potential to provide important structural insights to support condensed phase work on biological mixed-charge systems.[40−42]

2. Computational Method

Conformational searches were performed to generate 100 candidate structures using the Merk molecular force field (MMFF94) as implemented in SPARTAN. The default parameters were used including an initial temperature of 5000 K (the lowest 100 minima were saved).[43] The initial starting structures were refined using molecular mechanics based on the MMFF94 force field, prior to performing the conformational searches. Calculations were conducted for each of the four possible tautomers of $Na^+ \cdot [ATP\text{-}2H]^{2-}$ that are based on the four tautomers of $[ATP\text{-}2H]^{2-}$ (Figure 1). For $Na^+ \cdot [ATP\text{-}2H]^{2-}$, the fully optimized $[ATP\text{-}2H]^{2-}$ tautomer structures were used in the respective starting structures with the Na^+ placed close to the negatively charged phosphate groups. The initial cation position was not found to influence the final structures.

Single-point (sp) energies for the 50 lowest-energy MMFF94 conformers were obtained at the B3LYP/6-31+G* level using Gaussian 03.[44] Conformers were then manually inspected and grouped into "families" that display similar gross structures. The lowest-energy conformer from each family was then fully optimized (B3LYP/6-31+G*) to further refine the energy ordering of the families. Frequency calculations were conducted to ensure that the optimized structures correspond to true minima. Finally, MP2/6-31+G*(sp) energies were also obtained for the lowest conformer of each family for comparison against the B3LYP/6-31+G* relative energies. Using this strategy, a picture is built up of the most probable low-energy conformations. The approach described here is unique, but complements work by other groups toward a similar goal.[45−49]

We note that the methodology adopted here is unlikely to identify all of the low-energy conformers for the system under study, since it relies on the effectiveness of the MMFF94 force field. (It is not the goal of this work to evaluate or develop

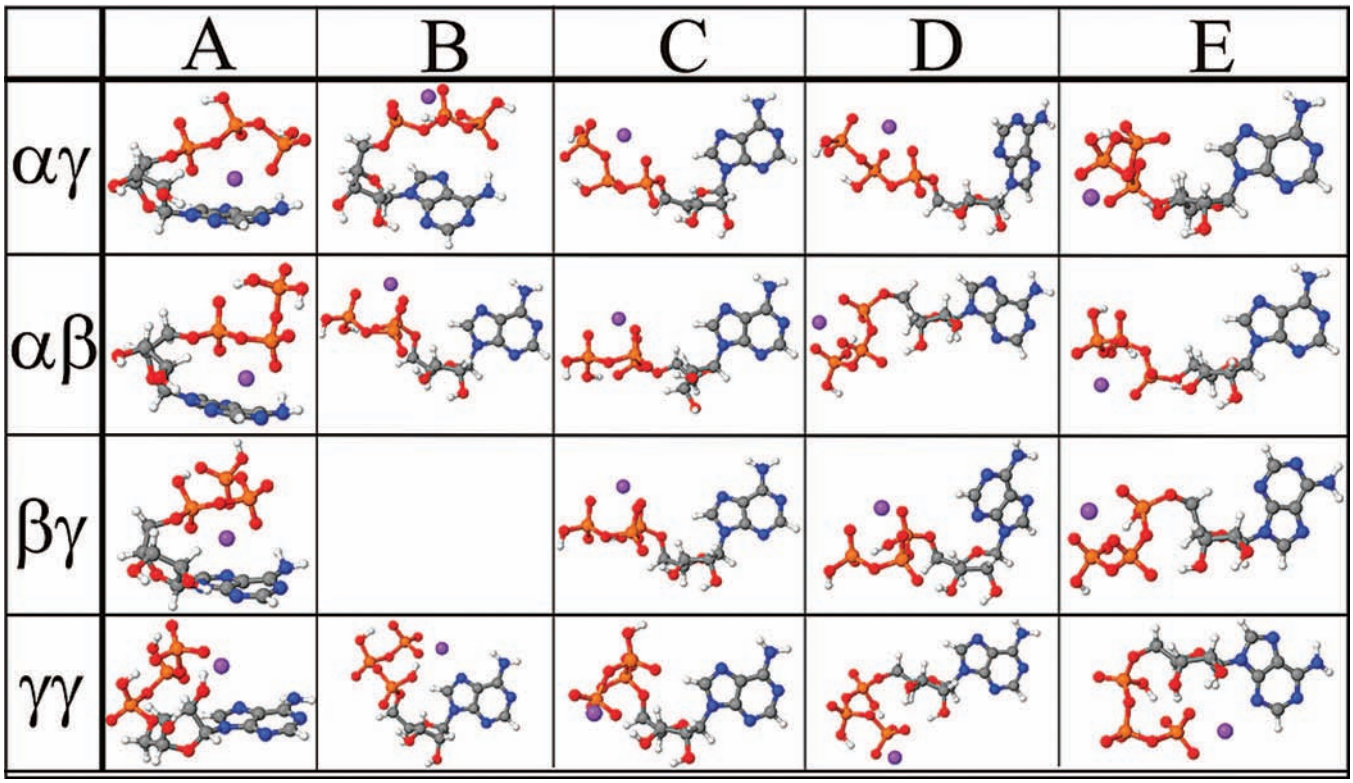

Figure 2. Illustration of the five structural families (A−E) of the four tautomers ($\alpha\gamma$, $\alpha\beta$, $\beta\gamma$, and $\gamma\gamma$) of $Na^+ \cdot [ATP\text{-}2H]^{2-}$. The structures displayed are the lowest energy optimized structures at the B3LYP/6-31+G* level. Note that none of the $\beta\gamma$-tautomer conformers inspected corresponded to a family B structure. The conformers are displayed with the ribose oriented the same way for each structure.

force fields, but to provide a method for proceeding from a set of molecular conformations to hierarachical calculations.) Kaminsky and Jensen have recently performed a study to evaluate the performance of a number of force fields against full MP2 calculations at calculating conformational isomers for four amino acids in model peptides.[45] MMFF94 was assessed to provide the best performance among the traditional fixed charge force fields (which included AMBER94, AMBER99, and OPLS), identifying ~60% of the MP2 conformations. They noted that the missing conformers tended to be the higher energy conformers.

3. Results and Discussion

3.1. $Na^+ \cdot [ATP\text{-}2H]^2$.

3.1a. Description of the Conformer Families for $Na^+ \cdot [ATP\text{-}2H]^{2-}$ and Overview of Structures. Figure 2 illustrates the conformer families (A−E) that describe the main structural variations of the four tautomers of $Na^+ \cdot [ATP\text{-}2H]^{2-}$. Inspection of the structures reveals that the Na^+ interacts directly with the negatively charged phosphates (maximum distance = 2.54 Å) in all of these low-energy conformers, while a number of the structures also display close cation−adenine interactions. For conformers of a given tautomer, it is notable that the specific interactions between the phosphate oxygens and the Na^+ are the same. The differences between families of a tautomer are therefore associated with the degree of interaction between the Na^+ and the adenine group, and the extent of the phosphate−adenine interactions. (Within a family of a tautomer, conformers vary only with respect to the phosphate−sugar or sugar−adenine torsional angles.)

In discussing the structures it is useful to define four key geometric parameters, namely, an intramolecular angle (P_α−O−N_9) between the phosphate−ribose−adenine groups and the closest distance of the cation from the adenine N_1, N_3, and N_7 nitrogen atoms (Figure 1a). Table 1 lists the values of these parameters for the lowest-energy conformer of each family of $Na^+ \cdot [ATP\text{-}2H]^{2-}$ (see below). The parameters are typical for conformers of the family. In general, the structures become less compact on going from family A to E, with the phosphate−ribose−adenine angle increasing across the series. The parameters listed in Table 1 illustrate that smaller cation−adenine distances are associated with the smaller phosphate−ribose−adenine angles, i.e., the more compact structures.

TABLE 1: Key Structural Parameters for the Lowest-Energy Conformers of $Na^+ \cdot [ATP\text{-}2H]^{2-}$ Illustrated in Figure 2

tautomer	family	angle[a]	N_7 distance[b]	N_1 distance[b]	N_3 distance[b]
$\alpha\gamma$	A	77.7	2.48	5.54	5.77
	B	82.9	4.96	7.80	7.56
	C	102.0	6.37	10.06	9.46
	D	124.1	9.64	7.84	6.87
	E	119.3	8.79	11.91	10.19
$\alpha\beta$	A	73.3	2.39	5.41	5.71
	B	98.8	6.48	9.99	9.31
	C	151.0	10.89	13.90	12.07
	D	135.0	11.29	13.54	11.33
	E	108.7	6.86	10.44	9.31
$\beta\gamma$	A	76.1	2.59	5.60	5.88
	C	100.0	6.48	9.93	9.26
	D	112.8	8.79	6.24	5.51
	E	145.3	11.84	11.54	9.29
$\gamma\gamma$	A	100.7	2.52	5.33	5.21
	B	89.4	2.34	5.72	5.96
	C	107.5	8.78	11.82	10.31
	D	165.0	5.88	11.12	8.83
	E	152.7	10.07	4.64	2.52

[a] Intramolecular angle (P_α−O−N_9, in degrees) between the phosphate−ribose−adenine groups. [b] Distance (in Å) of Na^+ from N_7, N_1, and N_3 of adenine (Figure 1a), respectively.

In group A, the $[ATP\text{-}2H]^{2-}$ dianion surrounds the Na^+ creating highly compact conformers. These structures correspond to the Na^+ binding above the plane of the electron-rich adenine ring and simultaneously binding to the anionic phosphates. There are also additional direct phosphate−adenine interactions (in the $\alpha\gamma$-, $\alpha\beta$-, and $\beta\gamma$-tautomers) which are associated with distortion of the adenine away from a planar geometry. In addition to the hydrogen bonds within the phosphate chain, there are additional hydrogen-bonding interactions between the sugar ring and the adenine (in the $\alpha\gamma$-, $\alpha\beta$-, and $\beta\gamma$-tautomers). We note that the $\gamma\gamma$-tautomer structure is somewhat distinctive as it does not share these interactions with the other family A tautomer structures. This trend also occurs for the other families and relates to the unique molecular conformations that are associated with the doubly deprotonated terminal phosphate.

The distinctive structural feature of the group B conformers is the presence of a close (<3.5 Å) α-phosphate|N_9-adenine interaction. These interactions again result in compact conformations, although the structures are slightly more open than for family A.

The most compact structures of $Na^+ \cdot [ATP\text{-}2H]^{2-}$ (family A $\alpha\gamma$-, $\alpha\beta$-, and $\beta\gamma$-tautomers, and the family B $\alpha\gamma$-tautomer) display hydrogen-bonding interactions between the sugar ring and the adenine, but also between the adenine NH_2 and phosphates. These compact structures are favorable primarily because the cation is able to simultaneously interact with the phosphate and adenine, but also because the acute angle geometry facilitates these additional hydrogen-bonding interactions.

The family C conformers have the Na^+ primarily interacting with the phosphate chain. Within this family, the $[ATP\text{-}2H]^{2-}$ backbone is oriented so that the cation is bound to the phosphate with the adenine angled toward the cation. The family E conformers display the opposite situation with the Na^+ and adenine lying on opposite sides of the $[ATP\text{-}2H]^{2-}$ backbone. Finally, the family D conformers are the most linear structures, with no phosphate−adenine interactions. The family C−E conformers are considerably less compact than the family A and B conformers and share a number of common structural motifs with those seen in conformations of bare $[ATP\text{-}2H]^{2-}$ (section 3.2). The family E conformers of the $\gamma\gamma$-tautomer are again an exception among this group of conformers since they display direct Na^+ adenine interactions (~2.5 Å). (Note that these structures are still distinct from the family A $\gamma\gamma$-tautomer conformers because the Na^+ is *not* bound above the adenine plane.)

3.1b. Energies of the $Na^+ \cdot [ATP\text{-}2H]^{2-}$ Conformers: Comparing the Single-Point and Optimized Energies. Figure 3a displays a plot of the MMFF94 energy distribution of the $Na^+ \cdot [ATP\text{-}2H]^{2-}$ conformers, labeled according to their tautomeric species. The figure illustrates that the lowest-energy MMFF94 tautomer is the $\gamma\gamma$-species, with the other tautomers lying significantly higher in energy ($\alpha\gamma < \alpha\beta < \beta\gamma$). It is notable that the four tautomers are clearly separated in energy. However, the relative ordering of the $Na^+ \cdot [ATP\text{-}2H]^{2-}$ tautomers changes dramatically at the B3LYP/6-31+G* (sp) level, as illustrated in Figure 3b. (The B3LYP results are assumed to be more reliable than the MMFF94 results through this discussion, since they are quantum mechanical energies rather than simple molecular mechanics. For a recent comparison, readers are referred to ref 45.) In contrast to the MMFF94 energy plot, the $\gamma\gamma$-species is now the highest energy tautomer, with the other tautomers lying significantly lower in energy. (The poor performance of the MMFF94 force field for the $\gamma\gamma$-tautomer is likely a result of the fact that none of the systems included in the core parametrization of MMFF94 have two excess charges on one functional group.[50]) There is some overlap between the energies of the $\alpha\beta$-, $\beta\gamma$-, and $\alpha\gamma$-tautomer conformers, with the general energy ordering being $\beta\gamma < \alpha\beta < \alpha\gamma$.

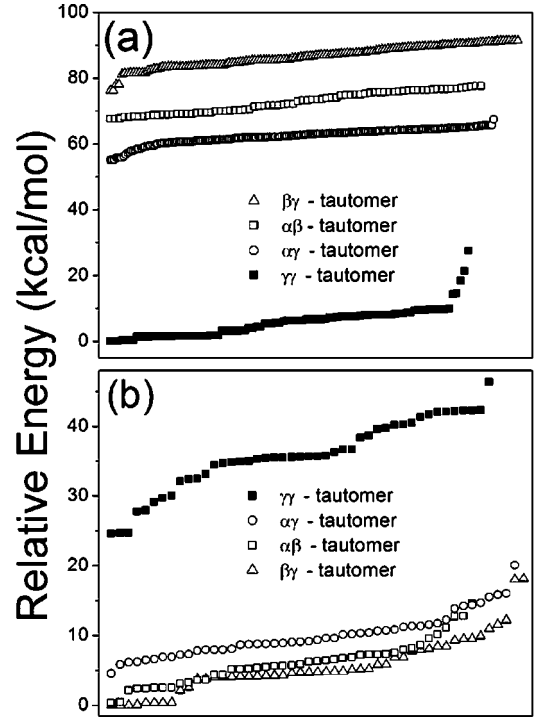

Figure 3. Energy distribution plots (relative energies in kcal/mol) for the conformers of $Na^+ \cdot [ATP\text{-}2H]^{2-}$ labeled according to tautomeric species: (a) MMFF94 energies (100 lowest-energy conformers), and (b) B3LYP/6-31+G*(sp) energies (50 lowest-energy conformers).

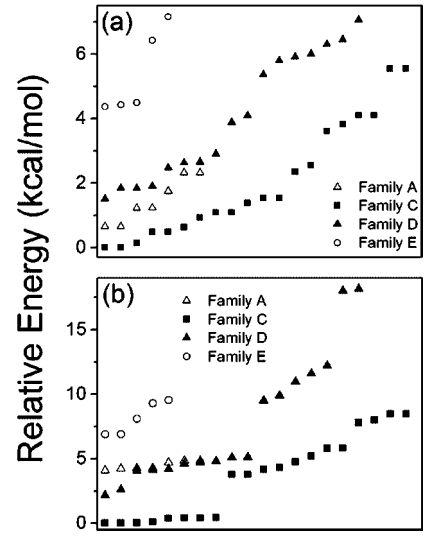

Figure 4. Energy distribution plots (relative energies in kcal/mol) for the $\beta\gamma$-tautomer conformers of $Na^+ \cdot [ATP\text{-}2H]^{2-}$ labeled according to family: (a) MMFF94 energies and (b) B3LYP/6-31+G*(sp) energies.

Figure 4a displays a plot of the MMFF94 energy distribution of just the $\beta\gamma$-tautomers labeled according to family. The family C conformers correspond to the lowest-energy conformations, with the compact family A structures lying next in energy. Figure 4b displays the corresponding plot of the B3LYP/6-31+G*(sp) energies for the $\beta\gamma$-tautomer. It is notable that the relative ordering of the families of conformers is reasonably

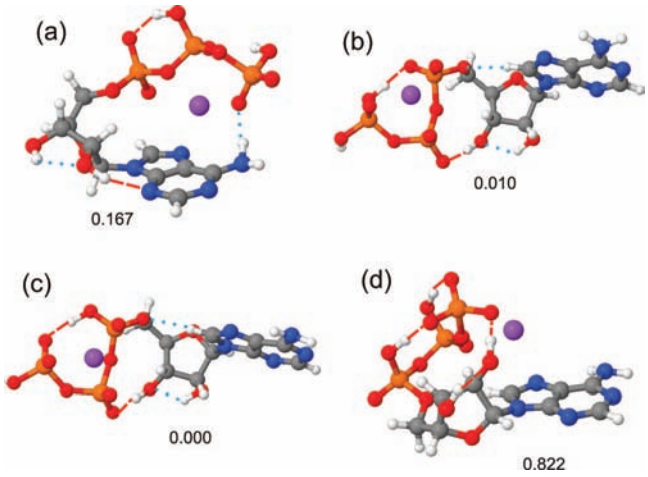

Figure 5. Optimized geometric structures (B3LYP/6-31+G*) of the lowest-energy conformational minima of the (a) $\alpha\gamma$-tautomer (family A conformer), (b) $\alpha\beta$-tautomer (family B conformer), (c) $\beta\gamma$-tautomer (family C conformer), and (d) $\gamma\gamma$-tautomers (family A conformer) of $Na^+ \cdot [ATP\text{-}2H]^{2-}$. The relative energies (in eV) are included on the figure. Typical hydrogen bonds are indicated as red dashed lines, with "loose" hydrogen-bond-like interactions as blue dotted lines.[51]

consistent on going from MMFF94 to B3LYP/6-31+G*(sp), with the family C structures lying lowest in energy, followed by the family A structures. Furthermore, both energy plots show the family A and family D conformers appearing with broadly similar energy, with the family E conformers being the highest energy structures. Similar results were obtained for the other tautomer families.

One of the most notable features of the presentation of the data points displayed in Figure 4b (and for the related data presented for $[ATP\text{-}2H]^{2-}$ in Figure 8b) is the clustering of data points within families, and the associated energy steps. The data point clusters are associated with "subfamilies" of structures, so that the energy steps correspond to modest structural changes. For example, for the family D structures, the energy step between the lowest cluster of data points to the next group of data points (data point 2 → 3) corresponds to a small change in the orientation of the adenine group. From data point 10 → 11 there is a change in the phosphate−adenine angle resulting in a slightly more open structure, while from data point 15 → 16, the orientation of the phosphate chain becomes more curled back upon itself. We emphasize that none of these changes are significant enough to warrant reclassifying the structures into another family.

While the abundance of families of conformers for a given tautomer is not directly related to the energy ordering of the families in the straightforward molecular mechanics calculations performed here (this differs from an annealing calculation), it is of interest to consider the abundances. For the $\beta\gamma$-tautomer results which are presented in Figure 4, 14% of the conformers belong to family A, 41% belong to family C, 35% belong to family D, and 10% belong to family E. At the B3LYP/6-31+G*(sp) level (Figure 4b), the most abundant families of conformer (C and D) correspond to the lowest-energy structures.

Full geometry optimizations (B3LYP/6-31+G*) were performed for the lowest-energy conformer of each family of $Na^+ \cdot [ATP\text{-}2H]^{2-}$. The optimized structures of these 19 conformers are displayed in Figure 2. Figure 5 displays expanded views of the lowest-energy optimized conformational minima obtained for each tautomer, illustrating the hydrogen bonds present in each structure. The figure also illustrates the highly

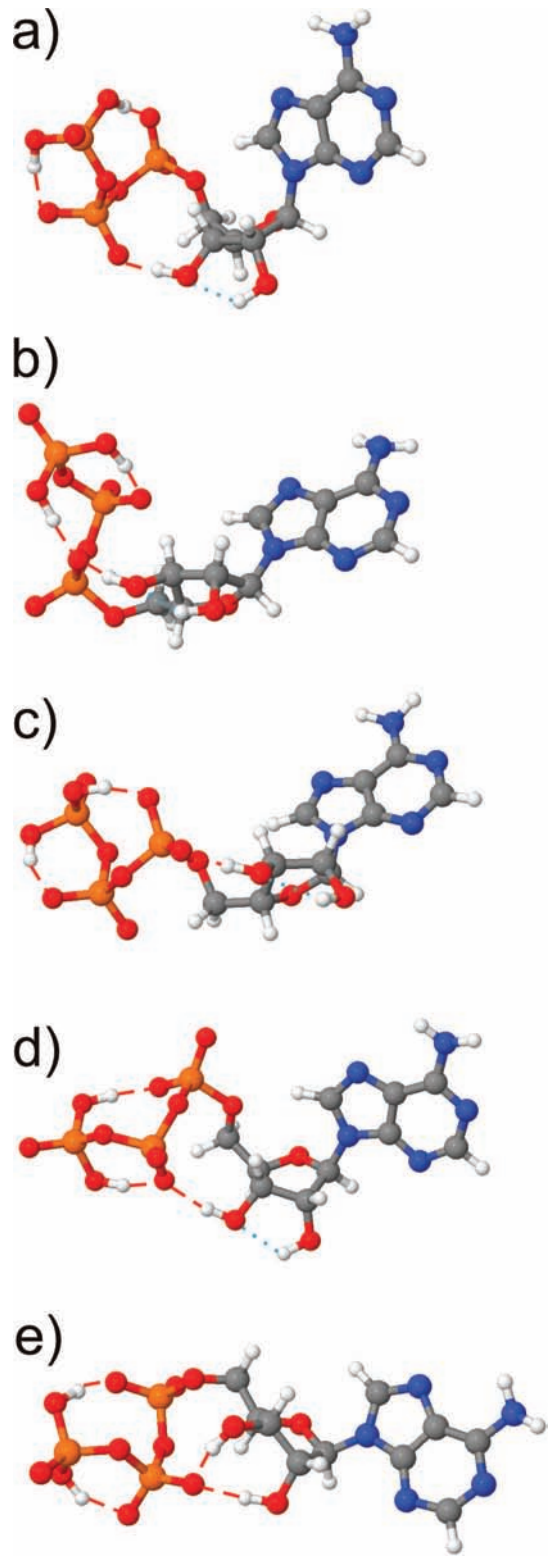

Figure 6. Geometric structures (MMFF94) of the $\alpha\beta$-tautomer of $[ATP\text{-}2H]^{2-}$ showing conformers from family (a) **a**, (b) **b**, (c) **c**, (d) **d**, and (e) **e**. Typical hydrogen bonds are indicated as red dashed lines, with "loose" hydrogen-bond-like interactions as blue dotted lines.[51]

similar structures of the lowest-energy conformers of the $\alpha\beta$-(Figure 5b) and $\beta\gamma$-tautomers (Figure 5c). These conformers differ by only one protonation site on the phosphate chain and the relative orientation of the adenine, sugar, and phosphate groups is highly similar (Table 1). Higher-level calculations would be necessary to establish a reliable energy ordering for these conformers.

TABLE 2: Relative Energies (B3LYP/6-31+G*(sp), B3LYP/6-31+G* Optimized, and MP2/6-31+G*(sp)//B3LYP/6-31+G*) for the Lowest-Energy Conformers of Each Structural Family of $Na^+ \cdot [ATP\text{-}2H]^{2-}$ Grouped According to Tautomer[a,b]

		B3LYP/6-31+G*(sp)		B3LYP/6-31+G*		MP2/6-31+G*(sp)[c]	
tautomer	family	ΔE^a/eV	ΔE^b/eV	ΔE^a/eV	ΔE^b/eV	ΔE^a/eV	ΔE^b/eV
$\alpha\gamma$	A	0.000	0.218	0.000	0.000	0.000	0.054
	B	0.419	0.626	0.321	0.321	0.386	0.435
	C	0.333	0.544	0.191	0.191	0.531	0.571
	D	0.272	0.490	0.382	0.382	0.714	0.762
	E	0.101	0.299	0.118	0.118	0.300	0.354
$\alpha\beta$	A	0.089	0.109	0.133	0.133	0.000	0.000
	B	0.000	0.027	0.000	0.000	0.136	0.136
	C	0.283	0.299	0.278	0.278	0.532	0.532
	D	0.12	0.136	0.085	0.085	0.299	0.299
	E	0.217	0.245	0.196	0.196	0.311	0.311
$\beta\gamma$	A	0.185	0.185	0.160	0.160	0.134	0.272
	C	0.000	0.000	0.000	0.000	0.000	0.136
	D	0.351	0.351	0.232	0.232	0.507	0.626
	E	0.093	0.093	0.080	0.080	0.099	0.218
$\gamma\gamma$	A	0.439	1.524	0.000	0.000	0.000	0.599
	B	0.000	1.088	n/a*	n/a*	n/a*	n/a*
	C	0.942	2.014	0.577	0.577	0.904	1.497
	D	0.765	1.850	0.603	0.603	0.908	1.497
	E	0.446	1.524	0.341	0.341	0.564	1.170

[a] Relative energy within tautomer. [b] Energy relative to the global minimum. For B3LYP (sp), ΔE is given relative to the family C conformer of the $\beta\gamma$-tautomer (absolute energy = −2828.085 H), for B3lYP (opt.) ΔE is given relative to the family C conformer of the $\beta\gamma$-tautomer (absolute energy = −2828.122 H), and for MP2 (sp), and ΔE is given relative to the family A conformer of the $\alpha\beta$-tautomer (absolute energy = −2821.766 H). [c] MP2/6-31+G*(sp)//B3LYP/6-31+G* energies. * This conformer converted to the $\alpha\gamma$-tautomer via proton transfer upon optimization and so the next lowest conformation, A, is taken as the minimum for the $\gamma\gamma$-tautomer.

Table 2 lists the B3LYP/6-31+G* energies for the fully optimized conformers, along with the corresponding zero-point-corrected energies and the relative conformer energies. A comparison of the absolute energies indicates that the lowest-energy conformers correspond to either $\alpha\beta$- or $\beta\gamma$-tautomers at both the single-point and fully optimized B3LYP/6-31+G* levels, with the $\gamma\gamma$-tautomers lying highest in energy. The relative energies of the families of conformers for a given tautomer are reasonably consistent on going from the single-point to the optimized energies. Table 2 also lists MP2/6-31+G*(sp)//B3LYP-6-31+G* energies for the $Na^+ \cdot [ATP\text{-}2H]^{2-}$ conformers, illustrating the important result that the lowest-energy conformers at the B3LYP/6-31+G* level, remain the lowest-energy conformers at the MP2/6-31+G*(sp) level within the expected accuracy of the calculations (~0.2 eV).

Focusing on the MP2/6-31+G*(sp) energies, it is evident that the lowest-energy structures tend to be the most compact conformers, i.e., a family A structure is the minimum for the $\alpha\gamma$-, $\alpha\beta$-, and $\gamma\gamma$-tautomers, with a family C structure (the second most compact for this tautomer) being the lowest-energy conformer for the $\beta\gamma$-tautomer.

3.1c. Geometric Changes of the $Na^+ \cdot [ATP\text{-}2H]^{2-}$ Conformer Structures upon Optimization. Upon optimization, the conformations of the $Na^+ \cdot [ATP\text{-}2H]^{2-}$ tautomers presented in Figure 2 changed remarkably little from the MMFF94-generated structures, with the overall family classification remaining unchanged, along with the hydrogen-bonding and ionic interactions. The main conformational changes that took place involved the adenine, which underwent modest changes including the ring planarity, the NH_2 planarity, and the adenine−sugar torsional angle. Group D and E structures became slightly less compact (the adenine group moved a maximum of 0.2 Å away from phosphate), and the adenine which was previously more perpendicular to the phosphate chain became more oriented toward it. The group A structures became slightly more compact, with the adenine becoming less planar (particularly for the $\alpha\beta$-tautomer).

The computed harmonic vibrational frequencies of the lowest-energy conformer of each of the four tautomers of $Na^+ \cdot [ATP\text{-}2H]^{2-}$ (Figure 5) is available in the Supporting Information (Table 1S), along with frequencies for the lowest-energy conformers of $[ATP\text{-}2H]^{2-}$. Vibrational frequencies are available for all of the conformers displayed in Figure 2 on request. The calculated frequencies indicate that the conformers display distinctive patterns of vibrational frequencies that should allow them to be identified using IR spectroscopy.

3.2. $[ATP\text{-}2H]^{2-}$. Calculated geometric structures for $[ATP\text{-}2H]^{2-}$ were presented in an earlier paper to aid the interpretation of collision-induced dissociation measurements.[22] However, full details of the calculations were not given and are therefore described here to illustrate the methodology for a second system. For $[ATP\text{-}2H]^{2-}$, the general method is the same as for $Na^+ \cdot [ATP\text{-}2H]^{2-}$ except that full optimizations (B3LYP/6-31+G*) were only carried out for the B3LYP/6-31+G*(sp) lowest-energy conformer of each tautomer.

3.2a. Description of the Conformer Families for $[ATP\text{-}2H]^{2-}$. In contrast to $Na^+ \cdot [ATP\text{-}2H]^{2-}$, the conformers of $[ATP\text{-}2H]^{2-}$ displayed more modest structural variation. For all of the $[ATP\text{-}2H]^{2-}$ conformers, the two sugar OH groups and the two protonated phosphate OH groups form hydrogen bonds with the rest of the triphosphate producing a cyclical arrangement for the phosphate chain.

Detailed inspection of the conformer structures, however, reveals that there is considerable variation in the number and type of hydrogen bonds, and these interactions were therefore used to classify $[ATP\text{-}2H]^{2-}$. The $\alpha\beta$-tautomer, for example, was classified into families as follows: this tautomer has four different OH groups (Figure 1b), labeled γOH_1 and γOH_2 (terminal phosphate groups), and OH_2 and OH_3 of the sugar. There are also five negatively charged $O^{\delta-}$ groups labeled γO_1 (terminal phosphate group), βO_1 and βO_2 (central phosphate group), and αO_1 and αO_2 (phosphate group nearest the sugar ring). The $\alpha\beta$-tautomer conformers each displays four of the following hydrogen-bonding interactions; $\gamma OH_1 \rightarrow \beta O_1$, γOH_2

TABLE 3: Hydrogen-Bonding Interactions Used To Define the Conformer Families of the αβ-Tautomer of $[ATP\text{-}2H]^{2-}$[a,b]

conformer family	hydrogen-bonding interactions			
a	$\gamma OH_1 \rightarrow \beta O_1$	$\gamma OH_2 \rightarrow \alpha O_1$	$OH_3 \rightarrow \beta O_2$	$OH_2 \rightarrow OH_3$
b	$\gamma OH_1 \rightarrow \beta O_1$	$\gamma OH_2 \rightarrow \alpha O_1$	$OH_3 \rightarrow \alpha O_1$	$OH_2 \rightarrow OH_3$
c	$\gamma OH_1 \rightarrow \beta O_1$	$\gamma OH_2 \rightarrow \alpha O_1$	$OH_3 \rightarrow \alpha O_2$	$OH_2 \rightarrow OH_3$
d	$\gamma OH_1 \rightarrow \beta O_1$	$\gamma OH_2 \rightarrow \alpha O_1$	$OH_3 \rightarrow \beta O_1$	$OH_2 \rightarrow OH_3$
e	$\gamma OH_1 \rightarrow \beta O_1$	$\gamma OH_2 \rightarrow \alpha O_1$	$OH_3 \rightarrow \beta O_2$	$OH_2 \rightarrow \beta O_2$

[a] H-bonds are listed from the most terminal OH group inward toward the sugar ring. [b] Representative structures are presented in Figure 6.

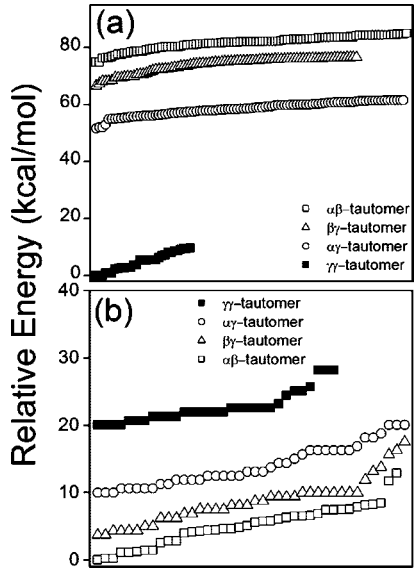

Figure 7. Energy distribution plots (relative energies in kcal/mol) for the conformers of $[ATP\text{-}2H]^{2-}$ labeled according to tautomeric species: (a) MMFF94 energies (100 lowest-energy conformers), and (b) B3LYP/6-31+G*(sp) energies (50 lowest-energy conformers).

$\rightarrow \alpha O_1$, $OH_3 \rightarrow \alpha O_1$, $OH_3 \rightarrow \alpha O_2$, $OH_3 \rightarrow \beta O_2$, $OH_3 \rightarrow \beta O_1$, $OH_2 \rightarrow OH_3$, and $OH_2 \rightarrow \beta O_2$. These hydrogen bonds include both "typical" hydrogen bonds and "loose" hydrogen-bond-like interactions.[51] Table 3 lists the hydrogen bonds for the resulting five conformer families (**a**−**e**), with representative structures presented in Figure 6. The same procedure was used for each tautomer, resulting in a specific list of hydrogen bonds for each conformer observed and hence a straightforward separation of the conformers into families.

3.2b. Energies of the $[ATP\text{-}2H]^{2-}$ Conformers: Comparing the Single-Point and Optimized Energies. Figure 7a displays a plot of the MMFF94 energy distribution of the 100 lowest-energy conformers of $[ATP\text{-}2H]^{2-}$ obtained from the initial conformer search, labeled according to their tautomeric species. The plot illustrates that, at the MMFF94 level, the lowest-energy tautomer is again the γγ-tautomer, with the other tautomers lying considerably higher in energy (αγ < βγ < αβ). The results mirror the Na^+•$[ATP\text{-}2H]^{2-}$ results since the energy variation between conformers of a tautomer is small relative to the energy difference between tautomers. The B3LYP/6-31+G* (sp) energy distribution for the $[ATP\text{-}2H]^{2-}$ conformers (labeled according to tautomer) is shown in Figure 7b. As in Na^+•$[ATP\text{-}2H]^{2-}$, γγ is the highest-energy tautomer compared to being the lowest-energy MMFF94 tautomer, with the overall tautomer ordering being αβ < βγ < αγ < γγ.

An MMFF94 energy plot of the αβ-tautomer conformers is displayed in Figure 8a, with the conformers labeled according

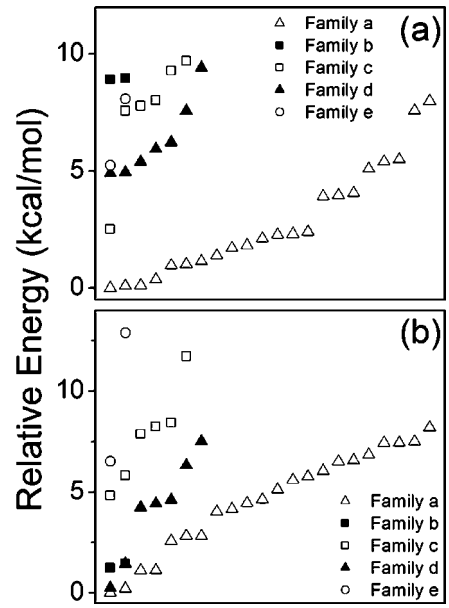

Figure 8. Energy distribution plots (relative energies in kcal/mol) for the αβ-tautomer conformers of $[ATP\text{-}2H]^{2-}$ labeled according to family: (a) MMFF94 energies and (b) B3LYP/6-31+G*(sp) energies.

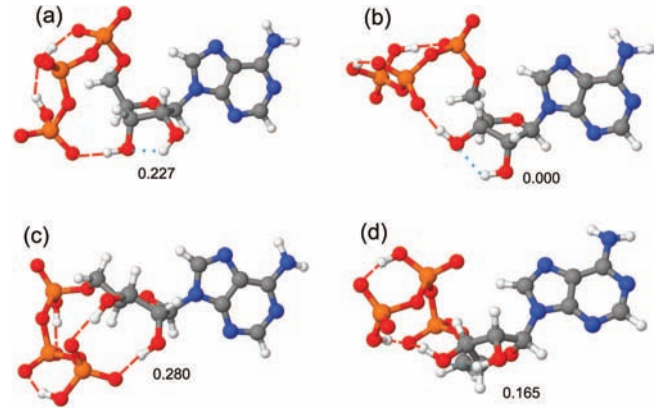

Figure 9. Optimized geometric structures (B3LYP/6-31+G*) of the lowest-energy conformational minima of the (a) αγ-tautomer (family **a** conformer), (b) αβ-tautomer (family **a** conformer), (c) βγ-tautomer (family **b** conformer), and (d) γγ-tautomers (family **b** conformer) of $[ATP\text{-}2H]^{2-}$. The B3LYP/6-31+G* relative energies are included on the figure. Typical hydrogen bonds are indicated as red dashed lines, with "loose" hydrogen-bond-like interactions as blue dotted lines.[51]

to family. Although there is some overlap in the energies of the different families, the family **a** structures display the lowest energies. The corresponding B3LYP/6-31+G* (sp) energy plot is displayed in Figure 8b. As in Na^+•$[ATP\text{-}2H]^{2-}$, it is notable that the relative ordering of the families is reasonably consistent on going from MMFF94 to B3LYP/6-31+G* (sp), with the family **a** structures again lying lowest in energy, followed by the family **d** structures. (We note that the most abundantly populated family, **a**, lies at the lowest energy in both the MMFF94 and B3LYP/6-31+G* (sp) plots.)

3.2c. Geometric Changes of the $[ATP\text{-}2H]^{2-}$ Conformer Structures upon Optimization. Full B3LYP/6-31+G* geometry optimizations were performed for the lowest-energy B3LYP/6-31+G*(sp) conformer of each tautomer. The optimized structures are displayed in Figure 9, with Table 4 listing the absolute, relative and zero-point-corrected energies. (Frequency calculations were conducted for these structures to ensure they are true minima. Selected IR vibrational frequencies obtained from the calculations are presented in Table 1S of the Supporting

TABLE 4: B3LYP/6-31+G*(sp), and B3LYP/6-31+G* Optimized Energies for the Lowest-Energy Conformers of the $[ATP\text{-}2H]^{2-}$ Tautomers[a]

	B3LYP-6-31+G*(sp)		B3LYP/6-31+G*	
tautomer	E/H	ΔE/eV	E[a]/H	ΔE/eV
$\alpha\gamma$	−2665.691	0.000	−2665.728 (−2665.422)	0.227 (0.273)
$\alpha\beta$	−2665.594	0.097	−2665.737 (−2665.432)	0.000 (0.000)
$\beta\gamma$	−2665.562	0.129	−2665.726 (−2665.420)	0.280 (0.327)
$\gamma\gamma$	−2665.588	0.103	−2665.731 (−2665.425)	0.165 (0.191)

[a] Zero-point-energy-corrected values are included in parentheses.

Information.) The lowest-energy conformer is an $\alpha\beta$-tautomer (Figure 9b), with the phosphate chain adopting a cyclic structure where the excess charges are stabilized by intramolecular hydrogen bonds. The primary hydrogen bonds connect γOH_1 to βO_1, γOH_2 to αO_1, and OH_3 of the ribose sugar to βO_2. Two additional weak hydrogen-bonding type interactions are also present. This low-energy structure was successfully used (along with structures for $[ATP\text{-}2H]^-$ and the related adenosine 5′-diphosphate anions) to provide a full interpretation of collision-induced dissociation measurements for this system.[22]

Overall, the conformeric structures changed very little upon optimization, with the specific hydrogen-bonding interactions and the gross structures remaining the same. Minor changes involved the bond lengths and angles along the phosphate chain, and the torsional angle of the adenine with respect to the sugar ring. The adenine remained planar, and oriented toward the phosphate chain, and the phosphate groups retained their cyclical hydrogen-bonding arrangement upon optimization. The distance between the phosphate groups and the adenine remained almost constant upon optimization, across the four tautomers.

3.3. Comparison of $[ATP\text{-}2H]^{2-}$ with $Na^+ \cdot [ATP\text{-}2H]^2$. In order to compare the structures of $[ATP\text{-}2H]^{2-}$ with those obtained for $Na^+ \cdot [ATP\text{-}2H]^{2-}$ in more detail, the $[ATP\text{-}2H]^{2-}$ conformations were separated into groups labeled A−E, based as closely as possible on the $Na^+ \cdot [ATP\text{-}2H]^{2-}$ families (section 3.1a). Figure 10 illustrates these $[ATP\text{-}2H]^{2-}$ structural groups allowing direct comparison with Figure 2. All of the $Na^+ \cdot [ATP\text{-}2H]^{2-}$ structures are considerably more compact than the bare $[ATP\text{-}2H]^{2-}$ structures, and there is much less structural variation among the $[ATP\text{-}2H]^{2-}$ conformations compared to $Na^+ \cdot [ATP\text{-}2H]^{2-}$. This is reflected in the B3LYP relative energies of the conformers of the two systems (Figures 3b and 7b), where the $Na^+ \cdot [ATP\text{-}2H]^2$ conformers have energies spread across 46 kcal/mol, compared to 28 kcal/mol for the $[ATP\text{-}2H]^{2-}$ conformers.

The hydrogen bonds within the phosphate chain are broadly similar in the sodiated and unsodiated tautomers, with similar structural motifs evident across the two systems, i.e., the cyclical arrangement of hydrogen bonds within the phosphate chain. This cyclical arrangement reflects the conformer structures adopted by the $H_3P_3O_{10}^{2-}$ triphosphate dianion.[14,22]

As discussed above, a number of the $Na^+ \cdot [ATP\text{-}2H]^{2-}$ structures have the Na^+ interacting with both the phosphate chain and the adenine. In the group A structures in particular, this double interaction (the Na^+ is typically ∼2.5 Å from the adenine) results in an acute phosphate−sugar−adenine angle conformation for the $[ATP\text{-}2H]^{2-}$ moiety within the cation−dianion complex (Table 1). No such "acute" angle structures were observed as low-energy conformers for $[ATP\text{-}2H]^{2-}$, since in the absence of the sodium cation, $[ATP\text{-}2H]^{2-}$ is able to maximize its noncovalent interactions without having to pay the energetic penalty associated with adopting the acute angle geometry. The conformers with the more acute phosphate−sugar−adenine angle display hydrogen-bonding interactions between the sugar and adenine groups, whereas conformers with more obtuse angles (including all the $[ATP\text{-}2H]^{2-}$ structures) have the sugar hydrogen bonding to the phosphate chain.

For the $Na^+ \cdot [ATP\text{-}2H]^{2-}$ structures, interactions exist between the phosphate chain and the adenine group, at the expense of hydrogen-bonding interactions between the phosphate chain and the sugar ring. There are no interactions between the phosphate chain and the adenine group for any of the $[ATP\text{-}2H]^{2-}$ structures, and the phosphate chain is always hydrogen bonded to one or both of the sugar OH groups. In $Na^+ \cdot [ATP\text{-}2H]^{2-}$, there are conformers where the OH groups on the phosphate chain are free, i.e., not hydrogen bonded (e.g., all structures of the $\alpha\beta$-tautomer). The $[ATP\text{-}2H]^{2-}$ OH groups, by contrast, are always hydrogen bonded. This is a direct result of the presence of strong cationic interactions in $Na^+ \cdot [ATP\text{-}2H]^{2-}$.

As noted above, the family C−E structures of $Na^+ \cdot [ATP\text{-}2H]^{2-}$ share a number of common structural motifs with those seen in conformations of bare $[ATP\text{-}2H]^{2-}$. However, the $Na^+ \cdot [ATP\text{-}2H]^{2-}$ complexes display relatively smaller distances between the phosphate and adenine groups, compared to $[ATP\text{-}2H]^{2-}$, indicating that the Na^+ strengthens these hydrogen-bonding interactions by polarizing the phosphate bonds.

4. Further Discussion

The only related study we are aware of to the work presented here is a molecular modeling investigation by Jin et al. of the preferred binding sites of Na^+ to negatively charged glycosaminoglycan disaccharides and tetrasaccharides.[23] The cations were found to significantly distort the sugar rings and to produce a greater variety of conformational structures than appear for the uncomplexed sugars. For the disaccharides, the cation acted as a bridge between the two sugar rings, simultaneously interacting with the two anionic sugar units. For the larger, more flexible tetrasaccharides, the sodiated structures were found to exhibit very compact structures. The calculations revealed that the Na^+ plays a vital role in reducing the Coulombic repulsion in these multiply charged species and hence enhances their gas-phase stability. The work of Jin et al. has very close parallels to our results, particularly in respect of the more varied structures obtained upon cation complexation. The "tightening" of the sugar complexes upon addition of Na^+ and the compact nature of our $Na^+ \cdot [ATP\text{-}2H]^{2-}$ structures are a direct result of the stabilization of the gas-phase species via the reduction of the Coulombic repulsion associated with the excess negative charges.

The $Na^+ \cdot [ATP\text{-}2H]^{2-}$ structures could be classified into families via a range of different criteria. It is important to emphasize that the main point of grouping structures into families is to ensure that structurally similar structures are not unnecessarily optimized in the hierarchical calculations. This provides a criterion for assessing different classification strategies, i.e., classification must group together conformers that display similar gross structures.

We initially attempted to classify the sodiated complexes by their hydrogen-bonding interactions, following the scheme described for $[ATP\text{-}2H]^{2-}$ in section 3.2a. However, it was immediately evident that the hydrogen bonds varied much less in the $Na^+ \cdot [ATP\text{-}2H]^{2-}$ conformers compared to $[ATP\text{-}2H]^{2-}$. Classification using hydrogen bonding resulted predominantly in just three families per tautomer (four for $\alpha\gamma$), but the "families" consisted of conformers that displayed very different gross structures. (Similar gross-structure conformers appeared

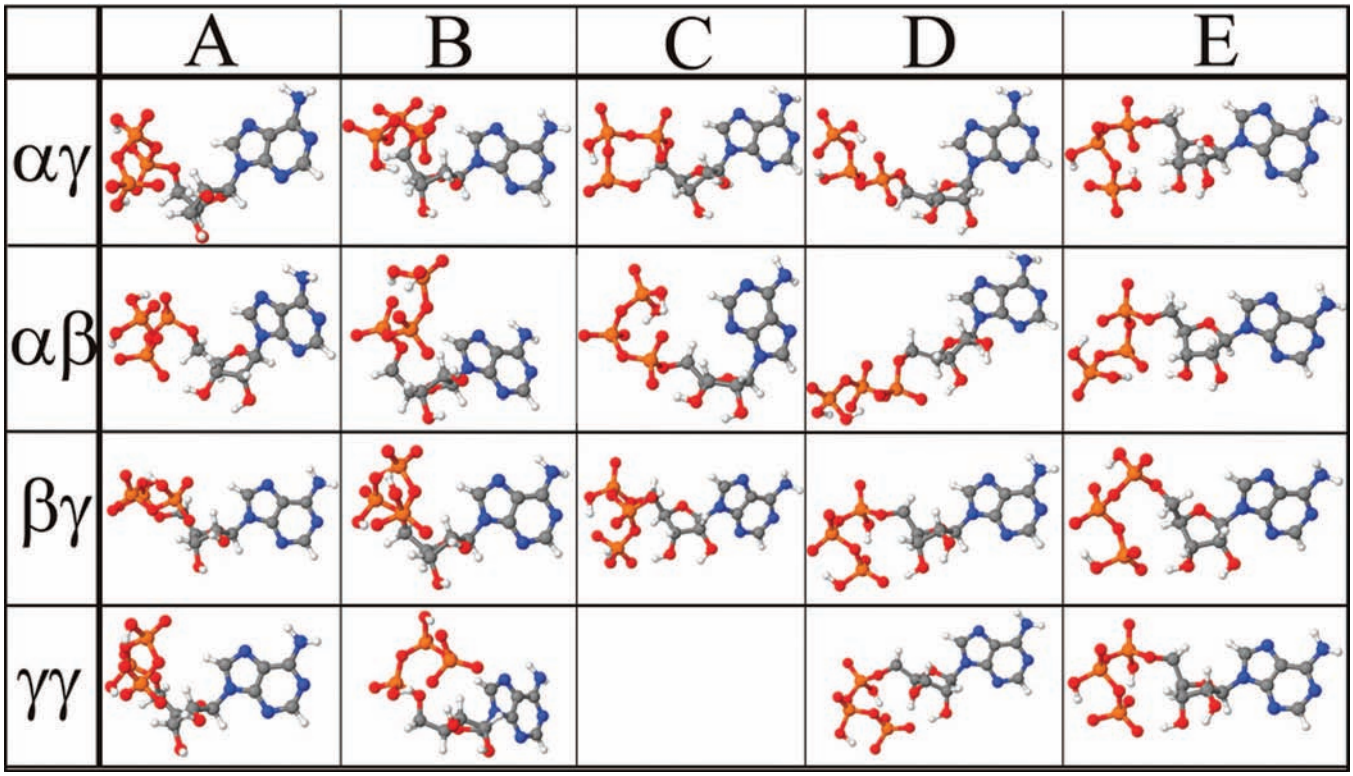

Figure 10. Table illustrating the five structural groups (A−E) of the four tautomers ($\alpha\gamma$, $\alpha\beta$, $\beta\gamma$, and $\gamma\gamma$) of $[ATP\text{-}2H]^{2-}$ for comparison with the corresponding table of structures for $Na^+ \cdot [ATP\text{-}2H]^{2-}$ given in Figure 2. The structures displayed are the MMFF94 structures and are shown with the ribose oriented the same way for each structure (as in Figure 2).

in different families; e.g., for $\alpha\gamma$ the family B, D, and E conformers displayed in Figure 2 appeared in a single family following classification just by hydrogen-bonding.)

Given the dominance of the cationic interactions within $Na^+ \cdot [ATP\text{-}2H]^{2-}$, the structures could also be classified via analysis of the cation binding sites. The Na^+ associates closely with the negatively charged phosphate chain in all of the conformers, but interacts with the electron-rich adenine to varying degrees. There are primary binding sites of Na^+ to adenine associated with the N_1, N_3, and N_7 nitrogens,[53] suggesting that the conformers could be grouped according to how closely the Na^+ was associated with each of these positions. However, this classification again resulted in families of structures consisting of conformers with very different gross structures. For example, although the Na^+-N_1, $-N_3$, and $-N_7$ distances for the lowest-energy family A and B conformers of the $\gamma\gamma$-tautomer are similar (Table 1), the Na^+ lies above the plane of the adenine ring for the family A conformers, but in the plane of the ring for the family B conformers. Ultimately, we resorted to inspecting the geometries manually and grouping them according to similar gross structures. The resulting families display characteristic noncovalent interactions, which are combinations of both hydrogen-bonding interactions and cation−phosphate and cation−adenine interactions. It would be of interest to analyze the noncovalent interactions within the resulting families of conformers quantitatively in future work.[54,21]

In conclusion, the structural variation (and hence classification) of the $Na^+ \cdot [ATP\text{-}2H]^{2-}$ conformers is more complex than for $[ATP\text{-}2H]^{2-}$, since the three-dimensional gas-phase structures adopted by the sodiated complex involve interplay between both cationic and hydrogen-bonding interactions. The number of hydrogen-bonding interactions is reduced in some of the conformer families to maximize the cationic interactions. However, the hydrogen bonds still play a crucial role in controlling the overall conformation of the structures.

5. Concluding Remarks

The identification of the lowest-energy isomers for a conformationally flexible molecular system is a problem of intense current interest.[55] For certain experimental techniques, e.g., ion mobility measurements,[56] molecular dynamics simulations have proved successful at providing adequate geometric structures to allow a reliable interpretation of the data obtained. However, the current advances in gas-phase laser spectroscopy of larger molecular systems, including protonated and deprotonated polypeptides,[57,58] demand that higher-level calculations are performed to fully optimize the molecular geometries and provide vibrational frequencies. Such calculations are still restrictively expensive for the size of systems that are now spectroscopically accessible. It is, therefore, important to have a reliable methodology for selecting trial structures that are likely to represent low-energy conformations.

The method presented in this paper of grouping structures according to families of structures that display similar gross molecular structures ensures that a representative sample of conformational structures is retained for hierarchical analysis, while very similar conformational structures are eliminated. The hierarchical (B3LYP and MP2) calculations indicate that the MMFF94 energies for different tautomers can be unreliable: while the MMFF94 energies of $Na^+ \cdot [ATP\text{-}2H]^{2-}$ and $[ATP\text{-}2H]^{2-}$ indicated that the $\gamma\gamma$-tautomer conformers appeared at much lower energies than the other tautomers, our higher-level calculations revealed that these conformers in fact represented the highest-energy structures. This illustrates the problem with any hierarchical refinement if the initial energies are unreliable, and indicates the importance of sampling widely prior to refining

the energies. Our method attempts to circumvent this problem by not just sampling from the lowest-energy force-field structures, since we do not omit any unique structural types just because they initially appear to be higher in energy.

For the $Na^+ \cdot [ATP\text{-}2H]^{2-}$ and $[ATP\text{-}2H]^{2-}$ systems, the geometries obtained from the MMFF94 molecular mechanics simulations changed only very little upon full optimization. This finding is in line with results from a recent study by Kaminsky and Jensen who found that the MMFF94 force field performed well for a fixed-charge force field at providing geometries and relative energies for amino acid (mixed-charge) conformations.[45] Given that the conformer geometries of $Na^+ \cdot [ATP\text{-}2H]^{2-}$ change little upon B3LYP optimization, it would be reasonable for similar systems to proceed straight to MP2(sp) energies to select the low-energy conformers prior to full optimization, with the caveat that all molecular tautomers should be explored.

Acknowledgment. C.E.H.D. thanks the EPSRC for support from Grant EP/C51212X/1, the Royal Society for support from a Royal Society University Research Fellowship, and the ERC for support from grant 208589-BIOIONS. We are also grateful for the award of computer time at the Rutherford Appleton Laboratories under the auspices of the Computational Chemistry Working Party from grant Chem 459.

Supporting Information Available: Computed harmonic vibrational frequencies of the lowest-energy conformer of each of the four tautomers of $Na^+ \cdot [ATP\text{-}2H]^{2-}$. This material is available free of charge via the Internet at http://pubs.acs.org.

References and Notes

(1) Robertson, E. G.; Simons, J. P. *Phys. Chem. Chem. Phys.* **2001**, *3*, 1.
(2) Wyttenbach, T.; Bowers, M. T. *Top. Curr. Chem.* **2003**, *225*, 207.
(3) Barran, P. E.; Polfer, N. C.; Campopiano, D. J.; Clarke, D. J.; Langridge-Smith, P. R. R.; Langley, R. J.; Govan, J. R. W.; Maxwell, A.; Dorin, J. R.; Millar, R. P.; Bowers, M. T. *Int. J. Mass. Spectrom.* **2005**, *240*, 273.
(4) Nir, E.; Hunig, I.; Kleinermanns, K.; de Vries, M. S. *Phys. Chem. Chem. Phys.* **2003**, *5*, 4780.
(5) Gerhards, M.; Utenberg, C.; Gerlach, A.; Jensen, A. *Phys. Chem. Chem. Phys.* **2004**, *6*, 2682.
(6) Jarrold, M. F. *Acc. Chem. Res.* **1999**, *32*, 360.
(7) Xu, S. J.; Zheng, W. J.; Radisic, D.; Bowen, K. H. *J. Chem. Phys.* **2005**, *122*, 091103.
(8) Srebalus Barnes, C. A.; Clemmer, D. E. *J. Phys. Chem. A* **2003**, *107*, 10566.
(9) Wang, X.; Levy, D. H.; Rubin, M. B.; Speiser, S. *J. Phys. Chem. A,* **2000**, *104*, 6558.
(10) Porath, D.; Bezryadin, A.; de Vries, S.; Dekker, C. *Nature,* **2000**, *403*, 635.
(11) Ullrich, S.; Tarczay, G.; Tong, X.; Dessent, C. E. H.; Müller-Dethlefs, K. *Angew. Chem., Int. Ed.* **2002**, *41*, 166.
(12) Stearns, J. A.; Mercier, S.; Seaiby, C.; Guidi, M.; Boyarkin, O. V.; Rizzo, T. R. *J. Am. Chem. Soc.* **2007**, *129*, 11814.
(13) Desfrancois, C.; Abdoul-Carime, H.; Schermann, J. P. *J. Chem. Phys.* **1996**, *104*, 7792.
(14) Julian, R. R.; Beauchamp, J. L. *Int. J. Mass Spectrom.* **2003**, *227*, 147.
(15) Kamariotis, A.; Boyarkin, O. V.; Mercier, S. R.; Beck, R. D.; Bush, M. F.; Williams, E. R.; Rizzo, T. R. *J. Am. Chem. Soc.* **2006**, *128*, 905.
(16) Wiedemann, S.; Metsala, A.; Nolting, D.; Weinkauf, R. *Phys. Chem. Chem. Phys.* **2004**, *6*, 2641.
(17) Duncan, M. A. *Int. J. Mass Spectrom.* **2000**, *200*, 545.
(18) Stace, A. J. *Phys. Chem. Chem. Phys.* **2001**, *3*, 1935.
(19) Robertson, W. H.; Johnson, M. A. *Annu. Rev. Phys. Chem.* **2003**, *54*, 173.
(20) Keutsch, F. N.; Saykally, R. J. *Proc. Natl. Acad. Sci.* **2001**, *98*, 10533.
(21) Hobza, P.; Müller-Dethlefs, K. *Chem. Rev.* **2000**, *100*, 143.
(22) Burke, R. M.; Pearce, J. K.; Boxford, W. E.; Bruckmann, A.; Dessent, C. E. H. *J. Phys. Chem. A* **2005**, *109*, 9775.
(23) Jin, L.; Barran, P. E.; Deakin, J. A.; Lyon, M.; Uhrin, D. *Phys. Chem. Chem. Phys.* **2005**, *7*, 3464.
(24) Dunbar, R. C.; Polfer, N. C.; Oomens, J. *J. Am. Chem. Soc.* **2007**, *129*, 14562.
(25) Bush, M. F.; Oomens, J.; Saykally, R. J.; Williams, E. R. *J. Am. Chem. Soc.* **2008**, *130*, 6463.
(26) Burke, R. M.; Boxford, W. E.; Dessent, C. E. H. *J. Chem. Phys.* **2006**, *125*, 021105.
(27) Burke, R. M.; Boxford, W. E.; Dessent, C. E. H. *J. Chem. Phys.* **2007**, *126*, 064308.
(28) Wang, X. B.; Ding, C. F.; Nicholas, J. B.; Dixon, D. A.; Wang, L. S. *J. Phys. Chem. A* **1999**, *103*, 3423.
(29) Alexandrova, A. N.; Boldyrev, A. I.; Zhai, H. J.; Wang, L. S. *J. Chem. Phys.* **2005**, *122*, 054313.
(30) Dreuw, A.; Cederbaum, L. S. *J. Chem. Phys.* **1999**, *111*, 1467.
(31) Kim, H. I.; Beauchamp, J. L. *J. Phys. Chem. A* **2007**, *111*, 5954.
(32) Suits, A. G.; Hepburn, J. W. *Annu. Rev. Phys. Chem.* **2006**, *57*, 431.
(33) Grabowski, Z. R.; Rotkiewicz, K.; Rettig, W. *Chem. Rev.* **2003**, *103*, 3899.
(34) Dedonder-Lardeux, C.; Gregoire, G.; Jouvet, C.; Martrechard, S.; Solgardi, D. *; Chem. Rev.* **2000**, *100*, 4023.
(35) Krutchinsky, A. N.; Chait, B. T. *J. Am. Soc. Mass. Spectrom.* **2002**, *13*, 129.
(36) Sigel, H.; Tribolet, R.; Malini-Balakrishnan, R.; Martin, R. B. *Inorg. Chem.* **1987**, *26*, 2149.
(37) Sigel, H.; Bianchi, E. M.; Corfu, N. A.; Kinjo, Y.; Tribolet, R.; Martin, R. B. *J. Chem. Soc., Perkin Trans. 2* **2001**, 507.
(38) Sigel, H.; Griesser, R. *Chem. Soc. Rev.* **2005**, *34*, 875.
(39) Sigel, H. *Pure Appl. Chem.* **2004**, *76*, 375.
(40) Perutz, M. F. *Science* **1978**, *201*, 1187.
(41) Koehl, P. *Curr. Opin. Strut. Biol.,* **2006**, *16*, 142.
(42) Sigel, R. K. O.; Pyle, A. M. *Chem. Rev.* **2007**, *107*, 97.
(43) Deppmeier, B. J.; Driessen, A. J. Hehre, T. S.; Hehre, W. J.; Johnson, J. A.; Klunzinger, P. E.; Leonard, J. M.; Ohlinger, W. S.; Pham, I. N.; Pietro, W. J.; Yu, J. *PC Spartan Pro*; Wavefunction, Inc.: Irvine, CA, 2000.
(44) Frisch, M. J.; et al. *Gaussian 03, Revision C.01*; Gaussian, Inc.: Pittsburgh, PA, 2003.
(45) Kaminsky, J.; Jensen, F. *J. Chem. Theory. Comput.* **2007**, *3*, 1774.
(46) Toroz, D.; van Mourik, T. *Mol. Phys.* **2006**, *104*, 559.
(47) Liu, D. F.; Wyttenbach, T.; Bowers, M. T. *J. Am. Chem. Soc.* **2006**, *128*, 15155.
(48) Bush, M. F.; O'Brien, J. T.; Prell, J. S.; Saykally, R. J.; Williams, E. R. *J. Am. Chem. Soc.* **2007**, *129*, 1612.
(49) Zwier, T. S. *J. Phys. Chem. A* **2006**, *110*, 4133, and references therein.
(50) Halgren, T. A. *J. Comput. Chem.* **1996**, *17*, 490.
(51) The term "hydrogen bond" is applied to any pairwise interaction between an electron-donating atom and an electron-pair-accepting hydrogen atom.[52] We define typical hydrogen bonds as having bond lengths <3 Å and angles of 180° ± 25°, with loose "hydrogen-bond-like" interactions having bond lengths <3.5 Å and angles of 180° ± 65°. A hydrogen bond typically has a length of ~2 Å and angles of 180°.
(52) Liu, D. F.; Wyttenbach, T.; Carpenter, C. J.; Bowers, M. T. *J. Am. Chem. Soc.* **2004**, *126*, 3261.
(53) Rodgers, M.; Armentrout, P. B. *J. Am. Chem. Soc.* **2000**, *122*, 8548.
(54) Jeziorski, B.; Moszynski, R.; Szalewicz, K. *Chem. Rev.* **1994**, *94*, 1887.
(55) de Bakker, R. I. W.; Furnham, N.; Blundell, T. L.; DePristo, M. A. *Curr. Opin. Strut. Biol.* **2006**, *16*, 160.
(56) Wyttenbach, T.; Bowers, M. T. *Annu. Rev. Phys. Chem.* **2007**, *58*, 511.
(57) Stearns, J. A.; Boyarkin, O. V.; Rizzo, T. R. *Chimia* **2008**, *62*, 240.
(58) Joly, L.; Antoine, R.; Broyer, M.; Lemoine, J.; Dugourd, P. *J. Phys. Chem. A* **2008**, *112*, 898.

JP805868U